

Heavy quarkonia in a contact interaction and an algebraic model: mass spectrum, decay constants, charge radii and elastic and transition form factors

Khépani Raya,¹ Marco A. Bedolla,^{1,2} J.J. Cobos-Martínez,^{3,4} and Adnan Bashir¹

¹ *Instituto de Física y Matemáticas, Universidad Michoacana de San Nicolás de Hidalgo, Edificio C-3, Ciudad Universitaria, Morelia, Michoacán 58040, México*

² *Istituto Nazionale di Fisica Nucleare (INFN), Sezione di Genova, via Dodecaneso 33, 16146 Genova, Italy*

³ *Laboratório de Física Teórica e Computacional,*

Universidade Cruzeiro do Sul, 01506-000 São Paulo, Brasil

⁴ *Cátedra CONACyT, Departamento de Física, Centro de Investigación y de Estudios Avanzados del Instituto Politécnico Nacional, Apartado Postal 14-740, 07000, Ciudad de México, México*

(Dated: December 31, 2021)

For the flavor-singlet heavy quark system of bottomonia, we compute the masses of the ground state mesons in four different channels, namely, pseudo-scalar ($\eta_b(1S)$), vector ($\Upsilon(1S)$), scalar ($\chi_{b0}(1P)$) and axial vector ($\chi_{b1}(1P)$). We also calculate the weak decay constants of the $\eta_b(1S)$ and $\Upsilon(1S)$ as well as the charge radius of $\eta_b(1S)$. It complements our previous study of the corresponding charmonia systems: $\eta_c(1S)$, $J/\Psi(1S)$, $\chi_{c0}(1P)$ and ($\chi_{c1}(1P)$). The unified formalism for this analysis is provided by a symmetry-preserving Schwinger-Dyson equations treatment of a vector \times vector contact interaction. Whenever a comparison is possible, our results are in fairly good agreement with experimental data and model calculations based upon Schwinger-Dyson and Bethe-Salpeter equations involving sophisticated interaction kernels. Within the same framework, we also report the elastic and transition form factors to two photons for the pseudo-scalar channels $\eta_c(1S)$ and $\eta_b(1S)$ in addition to the elastic form factors for the vector mesons J/Ψ and Υ for a wide range of photon momentum transfer squared (Q^2). For $\eta_c(1S)$ and $\eta_b(1S)$, we also provide predictions of an algebraic model which correlates remarkably well between the known infrared and ultraviolet limits of these form factors.

PACS numbers: 12.38.-t, 11.10.St, 11.15.Tk, 14.40.Lb

I. INTRODUCTION

The discovery of heavy and narrow J/ψ resonance in 1974 [1, 2] was followed by an even heavier and narrower Υ resonance in 1977 [3]. These systems are characterized by two diametrically opposite energy scales: the hard scale of the heavy constituent quark masses and the soft scale of the relative momenta between them. They are bound systems yet their diminishing size with increasing mass probes coupling which tends to approach asymptotic freedom. Schwinger-Dyson equations (SDEs) of quantum chromodynamics (QCD) provide a natural means to study these systems; their derivation makes no assumption about the strength of the interaction involved. Therefore, they are ideally suited to study systems or phenomena which probe different energy scales simultaneously.

Earliest studies of heavy quarkonia through SDEs can be traced back to Ref. [4]. With refined truncations of these equations and/or increased numerical complexity, these systems have also been investigated in Refs. [5–14]. Predictions for states with exotic quantum numbers were made in Refs. [15, 16].

The extension of this program to the complicated exotic and baryonic states, decay rates and form factors is considerably non-trivial. Brute force numerical evaluation stops short of exploring the large momentum transfer region of form factors and, at times, is unable to

make full comparison with already available experimental data. This shortcoming has been exposed in the calculation of elastic form factors (EFFs), see Ref. [17] for the pion EFF, as well as transition form factors (TFF), (see *e.g.*, Ref. [18] for the two photon TFF of η_c). However, an artful parameterization of the Bethe-Salpeter amplitudes (BSAs) in terms of Nakanishi-like perturbation theory integral representations [19] allows us to reach large space-like momentum transfer region, see for example Refs. [14, 20, 21].

A few years ago, an alternative to full QCD based explorations was put forward to study pion properties assuming that quarks interact, not via massless vector-boson exchange, but instead through a symmetry preserving vector-vector contact interaction (CI) [22–26]. One then proceeds by embedding this interaction in a rainbow-ladder (RL) truncation of the SDEs. Confinement is implemented by employing a proper time regularization scheme. This scheme systematically removes quadratic and logarithmic divergences ensuring the axial-vector Ward-Takahashi identity (axWTI) is satisfied. One can also explicitly verify the low energy Goldberger-Treiman relations. A fully consistent treatment of the CI model is simple to implement and can help us provide useful results which can be compared and contrasted with full QCD calculation and experiment.

This interaction is capable of providing a good description of the masses of meson and baryon ground and excited-states for light quarks [22–25]. The results de-

rived from the CI model are quantitatively comparable to those obtained using sophisticated QCD model interactions [15, 27–29]. Interestingly and importantly, this simple CI produces a parity-partner for each ground-state that is always more massive than its first radial excitation so that, in the nucleon channel, e.g., the first $J^P = 1/2^-$ state lies above the second $J^P = 1/2^+$ state [24, 30].

Considering the discussion so far as a satisfactory justification, in Ref. [31], we extended this interaction model to the sector of heavy quarkonia, computing the mass spectrum of charmonia as well as the decay constants of the pseudoscalar and vector meson channels. A subsequent publication [32] applies this model to the computation of the EFF and the TFF of the η_c . Low momentum limit of the form factors allows us to extract charge radii which compare well with the earlier SDE computations and the lattice results. A symmetry-preserving CI has also been employed recently to study charmed mesons in [33].

Building on our efforts, we now extend this interaction to the analysis of the flavor-singlet heavy quark system of bottomonia, computing the masses of the ground state mesons in four different channels: pseudo-scalar ($\eta_b(1S)$), vector ($\Upsilon(1S)$), scalar ($\chi_{b0}(1P)$) and axial vector ($\chi_{b1}(1P)$), as well as the *weak decay constants* of the $\eta_b(1S)$ and $\Upsilon(1S)$. We also compute the EFFs of $\eta_b(1S)$, J/ψ and $\Upsilon(1S)$, complementing our previous effort. Through evaluating the slope of these plots at the zero momentum transfer, we calculate and report their charge radii. We also calculate the transition form factor for $\eta_b \rightarrow \gamma^* \gamma$. Wherever possible, we compare our findings with experiment and/or other similar studies. Expectedly, the form factors are harder than we expect from the proper treatment of full QCD with a running quark mass function. As a quick fix, one resorts to the astutely constructed algebraic model (AM) and finds a near perfect substitute of cumbersome QCD based calculations.

The paper is organized as follows: in Section II we present the minimum but self contained details of the SDE-BSE approach to mesons; we also introduce the RL truncation for the CI and the consequences it has for the interaction kernels. We end the section by recalling the AM which mimics QCD to an adequate extent. In Section III, we tabulate our findings for the mass spectrum of the ground state bottomonia and decay constants of $\eta_b(1S)$ and $\Upsilon(1S)$. Section IV details algebraic expressions and numerical results for the EFFs of the pseudoscalar and vector mesons. It also contains a discussion on the quark-photon vertex we put to use, consistent with the WTI in the RL with a CI. Section V is devoted to the results and analysis of the transition form factors for the processes $\eta_{c(b)} \gamma^* \rightarrow \eta_{c(b)}$ and $\gamma \gamma^* \rightarrow \eta_{c(b)}$. Finally, in Section VI, we summarize our conclusions.

II. SDE-BSE FORMALISM

We devote this section to the brief recapitulation of the SDE-BSE formalism to study two-particle bound states and their connection with chiral symmetry breaking. Our particular focuss will naturally be on the CI which is employed to produce the bulk of results reported in this article.

A. The Gap Equation and the Contact Interaction

The f -flavor dressed-quark propagator S_f is obtained by solving the quark SDE [34–37]

$$S_f^{-1}(p) = i\gamma \cdot p + m_f + \Sigma_f(p), \quad (1)$$

$$\Sigma_f(p) = \int \frac{d^4 q}{(2\pi)^4} g^2 D_{\mu\nu}(p-q) \frac{\lambda^a}{2} \gamma_\mu S_f(q) \Gamma_\nu^a(p, q), \quad (2)$$

where g is the strong coupling constant, $D_{\mu\nu}$ is the dressed gluon propagator, Γ_ν^a is the dressed quark-gluon vertex, m_f is the f -flavor current-quark mass and λ^a are the usual Gell-Mann matrices.

Both $D_{\mu\nu}$ and Γ_ν^a satisfy their own SDEs, which in turn are coupled to higher n -point functions and so on *ad infinitum*. Therefore, the SDEs form an infinite set of coupled nonlinear integral equations, requiring a truncation scheme in order to define a tractable problem. This is achieved once we have specified the gluon propagator and the quark-gluon vertex. For a comprehensive recent review of the SDE-BSE formalism and its applications to hadron physics, see for example Refs. [27, 38].

The vector \times vector CI assumes that the force mediation among quarks takes place not via massless vector-boson exchange but instead through the interaction defined by:

$$g^2 D_{\mu\nu}(k) = \frac{4\pi\alpha_{\text{IR}}}{m_g^2} \delta_{\mu\nu} \equiv \frac{1}{m_G^2} \delta_{\mu\nu}, \quad (3)$$

$$\Gamma_\mu^a(p, q) = \frac{\lambda^a}{2} \gamma_\mu, \quad (4)$$

where $m_g = 800 \text{ MeV}$ is a gluon mass scale generated dynamically in QCD (see for example Ref. [39]) and α_{IR} is a parameter which specifies the enhanced interaction strength in the infrared (IR) [40, 41].

Equations (3) and (4) specify the kernel in the quark SDE, Eq. (1). In this truncation scheme, the general solution of the f -flavored dressed-quark propagator is immensely simplified [22–26, 31, 32]:

$$S_f^{-1}(p) = i\gamma \cdot p + M_f. \quad (5)$$

As the interaction, Eqs. (3,4), is momentum independent, the fermion mass M_f follows suit. This flavor-dependent constant mass is obtained by solving

$$M_f = m_f + \frac{16M_f}{3\pi^2 m_G^2} \int \frac{d^4 q}{(2\pi)^4} \frac{1}{q^2 + M_f^2}. \quad (6)$$

Since the integral in Eq. (6) is divergent, we must adopt a regularization procedure. We employ the proper time regularization scheme [42] to write this equation as

$$M_f = m_f + \frac{M_f^3}{3\pi^2 m_G^2} \Gamma(-1, \tau_{UV}^2 M_f^2, \tau_{IR}^2 M_f^2), \quad (7)$$

where $\Gamma(a, z_1, z_2)$ is the generalized incomplete Gamma function:

$$\Gamma(a, z_1, z_2) = \Gamma(a, z_1) - \Gamma(a, z_2).$$

The parameters τ_{IR} and τ_{UV} are, respectively, infrared and ultraviolet regulators. A nonzero value for $\tau_{IR} \equiv 1/\Lambda_{IR}$ implements confinement by ensuring the absence of quark production thresholds [43]. Since the CI is not a renormalizable theory, $\tau_{UV} \equiv 1/\Lambda_{UV}$ plays a dynamical role. Therefore, it sets the scale for all dimensioned quantities. The importance of an ultraviolet cutoff in Nambu–Jona-Lasinio type models has also been discussed in Refs. [44, 45].

Note that Eqs. (3,4) not only specify the kernel in the quark SDE, Eq. (1), but also the one in the BSE as we now make plain.

B. The BSE and the Contact Interaction

In quantum field theory, a meson bound state in a particular J^{PC} channel is described by the BSE [46–48]

$$[\Gamma_H(p; P)]_{tu} = \int \frac{d^4 q}{(2\pi)^4} K_{tu;rs}(p, q; P) \chi(q; P)_{sr}, \quad (8)$$

where $\chi(q; P) = S_f(q_+) \Gamma_H(q; P) S_g(q_-)$; $q_+ = q + \eta P$, $q_- = q - (1 - \eta)P$; $\eta \in [0, 1]$ is a momentum-sharing parameter, p (P) is the relative (total) momentum of the quark-antiquark system; $S_{f(g)}$ is the $f(g)$ -flavor dressed-quark propagator, already discussed; $\Gamma_H(p; P)$ is the meson Bethe-Salpeter amplitude (BSA), where H specifies the quantum numbers and flavor content of the meson; r, s, t , and u represent color, flavor, and spinor indices; and $K(p, q; P)$ is the quark-antiquark scattering kernel.

Eqs. (3,4) define and relate the kernel of the gap equation with that of the BSE, Eq. (8), through the axial-vector Ward-Takahashi identity (axWTI) [49]

$$-iP_\mu \Gamma_{5\mu}(k; P) = S^{-1}(k_+) \gamma_5 + \gamma_5 S^{-1}(k_-). \quad (9)$$

Eq. (9), which encodes the phenomenological features of dynamical chiral symmetry breaking in QCD, relates the axial-vector vertex, $\Gamma_{5\mu}(k; P)$, to the quark propagator, $S(k)$. This in turn implies a relationship between the kernel in the BSE, Eq. (8), and that in the quark SDE, Eq. (1). This relation must be preserved by any viable truncation scheme of the SDE-BSE coupled system, thus constraining the content of the quark-antiquark scattering kernel $K(p, q; P)$. For the CI, Eq. (9) implies

$$K(p, q; P) = -g^2 D_{\mu\nu}(p - q) \left[\frac{\lambda^a}{2} \gamma_\mu \right] \otimes \left[\frac{\lambda^a}{2} \gamma_\nu \right], \quad (10)$$

where $g^2 D_{\mu\nu}$ is given by Eq. (3). Thus, the homogeneous BSE ($\eta = 1$) takes the simple form

$$\Gamma_H(p; P) = -\frac{4}{3} \frac{1}{m_G^2} \int \frac{d^4 q}{(2\pi)^4} \gamma_\mu S_f(q+P) \Gamma_H(q; P) S_g(q) \gamma_\mu. \quad (11)$$

The axWTI further implies [22–26, 31, 32]

$$0 = \int_0^1 dx \int \frac{d^4 q}{(2\pi)^4} \frac{\frac{1}{2} q^2 + \mathfrak{M}^2}{(q^2 + \mathfrak{M}^2)^2}, \quad (12)$$

where

$$\mathfrak{M}^2 = M_f^2 x + M_g^2 (1 - x) + x(1 - x) P^2.$$

Eq. (12) has to be faithfully maintained during the entire calculation. It states that the axWTI is satisfied if, and only if, the model is regularized so as to ensure there are no quadratic or logarithmic divergences, circumstances under which a shift in integration variables is permitted. This is an essential requirement in order to prove Eq. (9) [22–25].

Since the interaction kernel of Eq. (10) does not depend on the external relative momentum, a symmetry-preserving regularization will return solutions which are independent of it. Therefore, the general forms of the BSAs for the pseudoscalar, scalar, vector, and axial-vector channels read, respectively:

$$\Gamma^{0-}(P) = \gamma_5 \left[iE^{0-}(P) + \frac{1}{2M} \gamma \cdot P F^{0-}(P) \right], \quad (13)$$

$$\Gamma^{0+}(P) = \mathbb{1} E^{0+}(P), \quad (14)$$

$$\Gamma_\mu^{1-}(P) = \gamma_\mu^T E^{1-}(P) + \frac{1}{2M} \sigma_{\mu\nu} P_\nu F^{1-}(P), \quad (15)$$

$$\Gamma_\mu^{1+}(P) = \gamma_5 \left[\gamma_\mu^T E^{1+}(P) + \frac{1}{2M} \sigma_{\mu\nu} P_\nu F^{1+}(P) \right] \quad (16)$$

where $M = M_f M_g / (M_f + M_g)$. The BSE is a homogeneous equation. Thus the BSA has to be normalized by a separate condition. In the RL approximation, this condition is:

$$1 = N_c \frac{\partial}{\partial P^2} \int \frac{d^4 q}{(2\pi)^4} \text{Tr} [\bar{\Gamma}_H(-Q) S(q+P) \Gamma_H(Q) S(q)], \quad (17)$$

evaluated at $Q = P$, where $P^2 = -m_H^2$, Γ_H is the normalized BSA of the meson H , and $\bar{\Gamma}_H$ is its charge-conjugated version. For the vector and axial-vector channels, there is an additional factor of 1/3 on the right-hand side to account for all three polarizations of a spin-1 meson.

Once the BSA has been canonically-normalized, we can extract observables with it. The pseudoscalar and vector leptonic decay constants, f_{0-} and f_{1-} , are defined, respectively, by

$$P_\mu f_{0-} = N_c \int \frac{d^4 q}{(2\pi)^4} \text{Tr} [\gamma_5 \gamma_\mu S(q_+) \Gamma_{0-}(P) S(q_-)], \quad (18)$$

$$m_V f_{1-} = \frac{N_c}{3} \int \frac{d^4 q}{(2\pi)^4} \text{Tr} [\gamma_\mu S(q_+) \Gamma_\mu^{1-} S(q_-)], \quad (19)$$

where m_V is the mass of the vector bound state, and the factor of 3 in the denominator corresponds to the three polarizations of the spin-1 meson.

C. The Algebraic Model

We present here a refined version of the previously employed AM for the heavy sector. For pseudoscalar mesons (of mass m_P), it reads as:

$$\Gamma_P(k; P) = i\gamma_5 \mathcal{N}_P \frac{M}{f_P} \int_0^1 dz \rho_\nu(z) \frac{M^2}{k^2 + z \sigma_P k \cdot P + M^2},$$

$$\rho_\nu(z) = \frac{1}{\sqrt{\pi}} \frac{\Gamma[\nu + 3/2]}{\Gamma[\nu + 1]} (1 - z^2)^\nu, \quad (20)$$

where \mathcal{N}_P is the canonical normalization constant, M is a mass scale (that we will relate to that of dynamical chiral symmetry breaking) and f_P is the weak decay constant; $\sigma_P \equiv m_\pi/m_P$ is defined such that the angular dependence, $k \cdot P$, decreases as the meson mass increases, and it recovers the algebraic model for the pion when $m_P = m_\pi$. We pick $\nu = 1$ in accordance with our earlier study of charmonia [32].

Since there is no experimental value of f_{η_b} , we choose $M = 4.818$ GeV. It is a reasonable value since the dynamically generated constituent-like mass generated by the CI is $M = 4.71$ GeV. Moreover, it produces the η_b weak decay constant which matches very well with the one reported in Ref. [13], based upon the most sophisticated SDE truncation so far. It is relevant to mention that this AM produces a finite-width delta-shaped parton distribution amplitude (PDA). Since this is the behavior of the PDA that one expects, one would also anticipate a decent prediction of the η_b form factors.

We now turn to the computation of physical observables in the following sections.

III. QUARKONIUM MASS SPECTRUM

In Ref. [31], we extended the CI model to charmonia. Our findings for the ground-state mass spectrum of quark-model mesons are presented in Table I; see Ref. [31] for a discussion of these results. In this work, we carry out an identical exercise for bottomonia. Table II displays results for the ground-state mass spectrum in four different channels, obtained by solving Eq. (11). It can be readily inferred from Table II that our results are in excellent agreement with the experimental data and those computed more sophisticated/complex models. That a RL truncation with a CI describes the mass spectrum of ground-state heavy-quarkonia, charmonia and bottomonia, so well can be easily understood because the quark wave function renormalization is strictly one and the mass function is momentum independent. It implies that the heavy-quark-gluon vertex can reasonably be approximated by its bare counterpart [31, 32].

	masses [GeV]			
	$m_{\eta_c(1S)}$	$m_{J/\Psi(1S)}$	$m_{\chi_{c0}(1P)}$	$m_{\chi_{c1}(1P)}$
Experiment [50]	2.983	3.096	3.414	3.510
CI [31]	2.976	3.09	3.374	3.4
JM [4]	2.821	3.1	3.605	-
BK [10]	2.928	3.111	3.321	3.437
RB [11]	3.065	-	-	-
FKW [12]	2.925	3.113	3.323	3.489
DGCLR [13]	2.98	3.07	-	-

TABLE I: The ground-state charmonia mass spectrum. The tabulated CI results were obtained with the best-fit parameter set: $m_g = 0.8$ GeV, $\alpha_{IR} = 0.93\pi/17 = 0.172$, $\Lambda_{IR} = 0.24$ GeV and $\Lambda_{UV} = 2.4$ GeV. Note that the two parameters which differ from the light sector are α_{IR} and Λ_{UV} for the reasons explained within the text. The current charm quark mass is $m_c = 1.09$ GeV, whereas the dynamically generated constituent-like mass is $M_c = 1.482$ GeV. The average percentage error, with respect to experimental data, is less than 3%. All subsequent calculation of charmonia related observables in this work employs the parameters listed in this table.

	masses [GeV]			
	$m_{\eta_b(1S)}$	$m_{\Upsilon(1S)}$	$m_{\chi_{b0}(1P)}$	$m_{\chi_{b1}(1P)}$
Experiment [50]	9.32 (9.4)	9.46	9.860	9.892
CI [This work]	9.345	9.460	9.594	9.603
JM [4]	9.322	9.460	9.860	—
BK [10]	9.405	9.488	9.831	9.878
FKW [12]	9.414	9.490	9.815	9.842
DGCLR [13]	9.39	9.46	-	-
MVRB [51]	-	9.552	-	-

TABLE II: Ground-state bottomonia mass spectrum. The CI results were obtained with the modified parameters $\alpha_{IR} = 0.93\pi/125 = 0.023$ and $\Lambda_{UV} = 6.4$ GeV. The current-quark mass is $m_b = 3.8$ GeV, and the dynamically generated constituentlike mass is $M_b = 4.7$ GeV. The average percentage error, with respect to experimental data, is again less than 3%. All bottomonia related observables in this work have been evaluated by using the parameters listed in this table.

The decay constants for the η_c and J/Ψ channels, computed in Ref. [31], are displayed in Table III, while the ones for the η_b and Υ channels, calculated in the present work, are tabulated in Table IV. Our results are in reasonably good agreement for charmonia with about 20% deviation. There is no experimental value available for f_{η_b} . However, our result for f_Υ does not fare very favorably against the one obtained with the most sophisticated analysis of the SDEs to date [13], with the deviation stretching up to around 50%.

As discussed at length in Ref. [31], we recall that the decay constant is influenced by the high momentum tail of the dressed-quark propagator and the BSAs [6, 57, 58], which probe the position space wave function of quarkonia at the origin. However, being momentum-independent, the CI results for the mass function and BSAs have no perturbative tail. This aspect is crucial

	decay constants [GeV]	
	f_{η_c}	$f_{J/\Psi}$
Experiment	0.238	0.294
CI [31]	0.255	0.206
Lattice QCD	0.279 [52]	0.286 [53]
BK [10]	0.282	0.317
KGH1 [54]	0.284	0.318
KGH2 [54]	0.267	0.291
DGCLR [13]	0.262	0.255
MVRB [51]	-	0.306

TABLE III: The decay constants for the states $\eta_c(1S)$ and $J/\Psi(1S)$. Note that the numerical values contain a division by $\sqrt{2}$ for a consistent comparison between different computations. The same is true for all subsequent discussion.

	decay constants [GeV]	
	f_{η_b}	f_{Υ}
Experiment	—	0.506
CI [This work]	0.553	0.219
Lattice QCD	0.472 [55]	0.459 [56]
BK [10]	0.501	0.486
KGH1 [54]	0.547	0.543
KGH2 [54]	0.535	0.500
DGCLR [13]	0.543	0.471

TABLE IV: The decay constants for the states $\eta_b(1S)$ and $\Upsilon(1S)$.

in a better prediction of the decay constants and would need to be built into the model in some indirect manner.

Moreover, as the quark masses become higher, mesons become increasingly pointlike in configuration space, thus weakening the interaction strength between their constituent quarks. It is this observation which led us to the natural extension of the CI model to heavy quarkonia by allowing a reduction of the effective coupling α_{IR} , accompanied by an appropriate increase in the ultraviolet cutoff Λ_{UV} . However, we have retained the parameters m_g and Λ_{IR} from the light sector. See Ref. [31], and references therein, for further discussion.

A. On the Choice of Parameters

quark	α_{IR}	Λ_{UV} [GeV]	α	Normalized
u, d, s	2.922	0.905	3.739	1
c	0.172	2.4	1.547	0.414
b	0.023	6.4	1.496	0.400

TABLE V: The parameters of coupling α_{IR} and Λ_{UV} are tabulated for different quark flavors. $m_g = 0.8 \text{ GeV}$ and $\Lambda_{IR} = 0.24 \text{ GeV}$ are the fixed parameters. We also provide explicit mass-scale dependent α given by Eq. (21). The last column yields its normalized value such that $\alpha = 1$ for the light quarks.

As mentioned previously, the only two parameters which are varied with the increasing quark masses are α_{IR} and Λ_{UV} . For the charmonia and bottomonia, these are determined from a best-fit to the mass and decay constant of the pseudoscalar channel. Those for the light-quarks sector were first obtained in Ref. [22, 24]. The arguments detailed earlier lead us to decrease α_{IR} with the increasing quark mass. This change has necessarily to be accompanied by a corresponding increase of Λ_{UV} to ensure we get the observed mass and decay constant of the pseudoscalar meson. One may ask if there is a quantitative pattern in the variation of α_{IR} and Λ_{UV} . In that case, a choice of Λ_{UV} will guide us towards the corresponding value of α_{IR} .

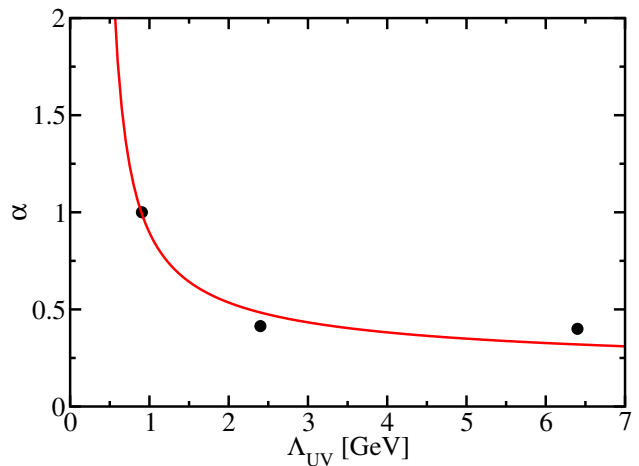


FIG. 1: Dimensionless coupling α for the contact interaction; see text. It is interesting to note that the variation of coupling α as a function of Λ_{UV} is not far from a logarithmic decrease fitted by the function $\alpha = a \log^{-1}(\Lambda_{UV}/\Lambda_0)$, where $\Lambda_0 = 0.357 \text{ GeV}$ and $a = 0.923$.

For this purpose, we define the following dimensionless coupling

$$\alpha = \alpha(\Lambda_{UV}) \equiv \frac{\alpha_{IR}}{m_g^2} \Lambda_{UV}^2. \quad (21)$$

The advantage of this definition is that α naturally varies with the mass scale Λ_{UV} . This variation is plotted in Fig. 1. The decrease of α , with respect to its value in the light-quarks sector, can be read off from the last column of Table V. Indeed, α is reduced by a factor of 2.1 – 2.3 in going from the light to the heavy sector (charmonia and bottomonia), instead of the apparent large factors quoted in Tables I and II. More importantly, we find out that the functional dependence of $\alpha(\Lambda_{UV})$ can be fitted reasonably well with an inverse logarithmic curve, reminiscent of the running QCD coupling with the momentum scale at which it is measured.

IV. ELASTIC FORM FACTORS

Despite the fact that the charge-conjugation eigenstates, such as quarkonia, do not have an EFF, we can still couple a vector current to their constituent quarks. We expect this exercise to yield valuable information about the internal structure of the state [32, 59]. Naturally, the vector current couples to the spin-1/2 quarks through the quark-photon interaction vertex. We briefly discuss this crucial ingredient in the following subsection.

A. The Quark-photon Vertex

It is of fundamental importance that quarks, whose dynamics inside hadrons is primarily dictated by QCD, also possess electromagnetic charge. The coupling of a photon with quarks plays an essential role in studying the internal structure of a hadron. Being an abelian theory, the only interaction of electromagnetic nature is the three-point quark-photon vertex.

The quark-photon vertex Γ_μ satisfies its own SDE and is constrained by the gauge invariance of QED through the vector Ward-Takahashi identity (WTI). Preserving this identity, and its $Q \rightarrow 0$ limit, is crucial to the conservation of electromagnetic current [17, 60]. With our treatment of the CI, the bare vertex γ_μ is sufficient to satisfy the WTI and ensure a unit value for the charged pion's electromagnetic form factor at zero momentum transfer. However, given the simplicity of the model, one can readily improve upon it. A vertex dressed consistently with our truncation is determined by the following inhomogeneous BSE, (see Refs. [22, 26, 32] for more details):

$$\Gamma_\mu(Q) = \gamma_\mu - \frac{4}{3m_G^2} \int \frac{d^4q}{(2\pi)^4} \gamma_\alpha \chi_\mu(q+P, q) \gamma_\alpha, \quad (22)$$

where $\chi_\mu(q+P, q) = S(q+P)\Gamma_\mu(Q)S(q)$. Therefore, the general form of the quark-photon vertex in the RL approximation with a CI is

$$\Gamma_\mu(Q) = \gamma_\mu^T P_T(Q^2) + \gamma_\mu^L P_L(Q^2), \quad (23)$$

where $Q_\mu \gamma_\mu^T = 0$ and $\gamma_\mu^T + \gamma_\mu^L = \gamma_\mu$. The SDE for $\Gamma_\mu(Q)$, Eq. (22), implies

$$P_L(Q^2) = 1, \quad (24)$$

$$P_T(Q^2) = \frac{1}{1 - K_V(Q^2)}, \quad (25)$$

as can be consulted in Ref. [26, 32]. $K_V(Q^2)$ is the BSE kernel in the vector channel, Eq. (15), within the present truncation scheme [31]. Therefore, because of the dressing of the quark-photon vertex through $P_T(Q^2)$, our results for the form factors (EFF and TFF) will develop a pole at $Q^2 = -m_V^2$, where m_V is the vector meson mass. Note that $P_T(Q^2 = 0) = 1$ and $P_T(Q^2 \rightarrow \infty) \rightarrow 1$,

leaving us with γ_μ , as expected, the latter being the statement that a dressed-quark becomes a current quark to a large- Q^2 probe.

B. η_c and η_b Elastic Form Factors

A pseudoscalar meson possesses just one vector current form factor $F_{\eta_{c(b)}}(Q^2)$, defined by the $\eta_{c(b)}\gamma^*$ vertex

$$\Lambda_\mu^{\eta_{c(b)}\gamma^*}(P_i, P_f; Q) = F_{\eta_{c(b)}}(Q^2)(P_i + P_f)_\mu, \quad (26)$$

where $Q = P_f - P_i$ is the virtual photon momentum and P_i (P_f) is that of the incoming (outgoing) meson. In our approach, the impulse approximation for the $\eta_{c(b)}\gamma^*$ vertex reads

$$\Lambda_\mu^{\eta_{c(b)}\gamma^*}(P, Q) = 2N_c \int \frac{d^4k}{(2\pi)^4} \text{Tr} [i\Gamma_{\eta_{c(b)}}(-P_f)S(k_2) i\Gamma_\mu(Q)S(k_1)i\Gamma_{\eta_{c(b)}}(P_i)S(k)], \quad (27)$$

where $\Gamma_\mu(Q)$ is the corresponding quark-photon vertex. Note that $P_f = P_i + Q$. We choose $P_i = P - Q/2$. Thus $P_f = P + Q/2$, $k_1 = k + P - Q/2$, and $k_2 = k + P + Q/2$. Since the scattering is elastic, $P_i^2 = P_f^2 = -m_{\eta_{c(b)}}^2$, which in turns implies $P \cdot Q = 0$ and $P^2 + Q^2/4 = -m_{\eta_{c(b)}}^2$, where $m_{\eta_{c(b)}}$ is the $\eta_{c(b)}$ mass.

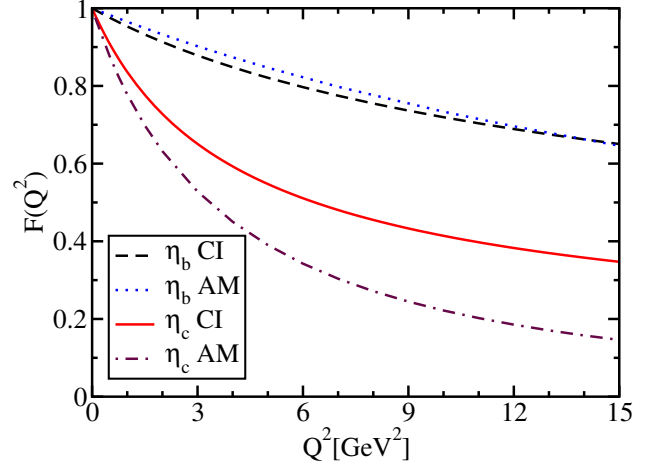


FIG. 2: We plot CI and AM results for the η_c and η_b EFFs. See Ref. [32] for a comparison between the CI result for the η_c EFF and that of lattice QCD from Ref. [59].

In Fig. 2, we display the η_c and η_b EFFs, calculated by using the dressed quark-photon vertex of Eq. (23). For heavy mesons, such as the η_c and the η_b , the dressing of the vertex has a negligible effect on the EFF; that is, in the CI, the bare vertex trivially satisfies the WTI. However, although the time-like sector has not been displayed

in Fig. 2, the $\eta_{c(b)}$ form factor has a pole at $Q^2 = -m_V^2$, the mass of the corresponding vector bound state; see Tables I and II. This is a consequence of appropriately dressing the quark-photon vertex. For heavy quarks, the vector-meson pole lies deep on the time-like axis and hence hardly affects the form factors for the space-like Q^2 . Wherever a comparison is possible, our results are harder than the ones predicted by the Lattice QCD [32]; see Ref. [32] for a detailed discussion.

Both for η_c and η_b , the EFFs cease to depend on Q^2 for its sufficiently large values. This is the characteristic behavior of a point-like particle. In fact, it is already known that the asymptotic form factors obtained with the CI are harder than those predicted by QCD [22, 23, 26, 32]. This is an inevitable consequence of the momentum independence of the interaction, Eq. (3). As compared to η_b , the η_c EFF increases more steeply for $Q^2 < 0$ since the pole (the J/Ψ pole for the η_c EFF) associated with the dressing of the c -quark-photon vertex lies closer to $Q^2 = 0$, naturally influencing the value of the charge radius defined as:

$$r_{\eta_{c(b)}}^2 = -6 \left. \frac{dF_{\eta_{c(b)}}(Q^2)}{dQ^2} \right|_{Q^2=0}. \quad (28)$$

Numerical values are presented in Table VI. The η_c charge radius compares well with the prediction from Lattice QCD [59]. The charge radii of η_c and η_b are also in reasonably good agreement with SDE results with more sophisticated Maris-Tandy model interaction [7, 61] and with a light-front quantized Hamiltonian model [62]. Clearly $r_{\eta_b} < r_{\eta_c}$, i.e., the heavier the meson, the closer it is to being a point particle.

charge radius (fm)			
	SDE	Lattice QCD	CI
η_c	0.219 [61]	0.25 [59, 63]	0.25 [32]
η_b	0.086 [7]	—	0.109 [This work]

TABLE VI: The charge radius for the state $\eta_{c(b)}(1S)$ with the CI, compared to some other computations.

C. J/Ψ and Υ elastic form factors

The electromagnetic structure of a spin-1 meson, like J/Ψ and Υ , is characterised by three vector current form factors [64]. We follow Ref. [61] in defining them.

$$\Lambda_{\lambda\mu\nu}^{V\gamma^*}(P, Q) = \sum_{i=1}^3 T_{\lambda\mu\nu}^i(P, Q) F_i(Q^2), \quad (29)$$

where $V = J/\Psi, \Upsilon$ and F_i , $i = 1, 2, 3$, are the EFFs. The kinematics remain identical to the case of pseudo-scalar particles. However, the masses now refer to those

of $M_{J/\Psi, \Upsilon}$. Defining the transverse projector

$$\mathcal{P}_{\mu\nu}^T(P) = \delta_{\mu\nu} - \frac{P_\mu P_\nu}{P^2}, \quad (30)$$

the tensors in Eq. (29) are [61]:

$$T_{\lambda\mu\nu}^1 = 2P_\lambda \mathcal{P}_{\mu\alpha}^T(P^i) \mathcal{P}_{\alpha\nu}^T(P^f), \quad (31)$$

$$T_{\lambda\mu\nu}^2 = \left[Q_\mu - P_\mu^i \frac{Q^2}{2m_V^2} \right] \mathcal{P}_{\lambda\nu}^T(P^f) - \left[Q_\nu + P_\nu^f \frac{Q^2}{2m_V^2} \right] \mathcal{P}_{\lambda\mu}^T(P^i), \quad (32)$$

$$T_{\lambda\mu\nu}^3 = \frac{P_\lambda}{m_V^2} \left[Q_\mu - P_\mu^i \frac{Q^2}{2m_V^2} \right] \left[Q_\nu + P_\nu^f \frac{Q^2}{2m_V^2} \right]. \quad (33)$$

A symmetry-preserving regularization scheme is crucial so that the following WTIs are preserved [26]

$$Q_\lambda \Lambda_{\lambda\mu\nu}^{V\gamma^*} = 0, \quad (34)$$

$$P_\mu^i \Lambda_{\lambda\mu\nu}^{V\gamma^*} = 0 = P_\nu^f \Lambda_{\lambda\mu\nu}^{V\gamma^*}. \quad (35)$$

The first equation follows from current conservation and the latter two simply reflect the fact that the massive vector meson is transverse.

A more convenient and physically relevant set [64] of form factors, known as the charge, magnetic dipole, and electric quadrupole form factors is given by

$$G_E(Q^2) = F_1(Q^2) + \frac{2}{3} \eta G_Q(Q^2), \quad (36)$$

$$G_M(Q^2) = -F_2(Q^2), \quad (37)$$

$$G_Q(Q^2) = F_1(Q^2) + F_2(Q^2) + (1 + \eta) F_3(Q^2), \quad (38)$$

where $\eta = Q^2/(4m_V^2)$. In the limit $Q^2 \rightarrow 0$, these form factors define the charge, magnetic dipole and electric quadrupole moments of the vector meson under consideration:

$$G_E(Q^2 = 0) = 1, \quad (39)$$

$$G_M(Q^2 = 0) = \mu, \quad (40)$$

$$G_Q(Q^2 = 0) = \mathcal{Q}. \quad (41)$$

For a point-like vector particle, the magnetic and quadrupole moments are $\mu = 2$ in units of $e/(2m_V)$ and $\mathcal{Q} = -1$ in units of e/m_V^2 , respectively [65].

In the impulse approximation the $V\gamma^*$ vertex can be calculated from the triangular configuration :

$$\Lambda_{\lambda\mu\nu}^{V\gamma^*}(P, Q) = 2N_c \int \frac{d^4k}{(2\pi)^4} \text{Tr} [\Gamma_\nu^V(-P^f) S(k + P^f) i\Gamma_\lambda(Q) S(k + P^i) \Gamma_\mu^V(P^i) S(k)] . \quad (42)$$

Hence if one uses a symmetry-preserving regularisation, $G_E(Q^2 = 0) = 1$ [26].

In Figures 3 and 4, we plot our results for G_E , G_M , and G_Q form factors for the vector mesons J/Ψ and Υ ,

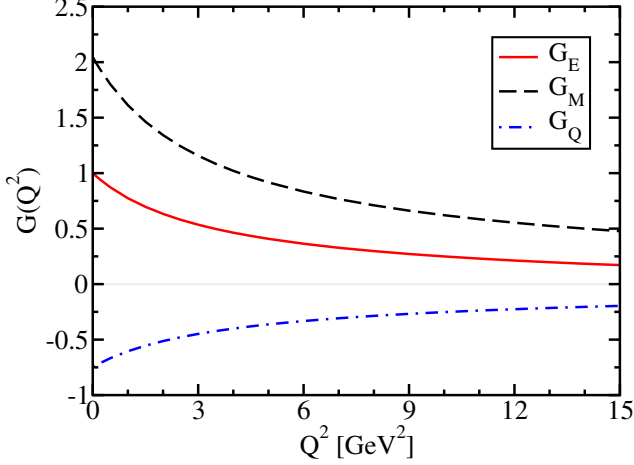


FIG. 3: Contact interaction results for the J/Ψ EFFs G_E , G_M , and G_Q .

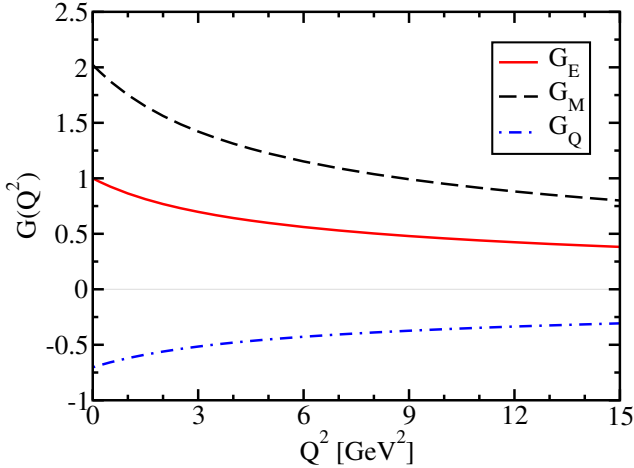


FIG. 4: Contact interaction plots for the Υ EFFs G_E , G_M , and G_Q .

respectively. As these form factors follow the same pattern as obtained for the ρ meson form factors in Ref. [26], the same analysis applies here. We would like to mention that as compared to the pseudoscalars, these form factors fall faster, as $1/Q^2$ for large Q^2 within the domain we explored, as opposed to the constant value observed for the pseudoscalars (see Fig. 2). This difference is due to the fact that the RL truncation with a CI prohibits the appearance of the vector component for the BSA of vector mesons, i.e., $F^{1-} = 0$ in Eq. (15). Asymptotic limit of QCD predicts [65]:

$$G_E(Q^2) : G_M(Q^2) : G_Q(Q^2) \xrightarrow{Q^2 \rightarrow \infty} 1 - \frac{2}{3}\eta : 2 : -1. \quad (43)$$

As noted in Ref. [26], this relation is recovered only for $\Lambda_{UV} \rightarrow \infty$ but spoils the convergence of integrals, implying that a vector-vector CI cannot be regularized in a simple manner consistent with the constraints of asymptotic QCD.

	r_E	r_M	r_Q	μ	Q
CI	0.262	0.254	0.240	2.047	-0.748
SDE [61]	0.228	-	-	2.13	-0.28
Lattice [59, 63]	0.257	-	-	2.10	-0.23

TABLE VII: Form factor radii (in fm) as well as magnetic and quadrupole moments for the J/Ψ meson.

	r_E	r_M	r_Q	μ	Q
CI	0.197	0.195	0.182	2.012	-0.704
SDE	-	-	-	-	-
Lattice	-	-	-	-	-

TABLE VIII: Form factor radii (in fm) as well as magnetic and quadrupole moments for the Υ meson.

In Tables VII and VIII, we present charge, magnetization and quadrupole radii, as well as magnetic, and quadrupole moments for the J/Ψ and Υ , respectively. Reiterating the fact that for a structureless spin-1 particle, $\mu = 2$ and $Q = -1$ [65] any deviations from these values point to the dynamics of the internal structure. From the tabulated results, we can infer that the heavy-mesons produced by the CI are nearly point-like, as they should be. Wherever comparison is possible, our results of Table VII are in very good agreement with those of SDEs and Lattice.

V. $\gamma\gamma^* \rightarrow \eta_{c(b)}$ TRANSITION FORM FACTOR

The interaction vertex describing the $\gamma\gamma^* \rightarrow \eta_{c(b)}$ transition can be parametrized by just one form factor $G_{\gamma\gamma^* \eta_{c(b)}}(Q_1^2, Q_2^2)$, which can be computed from

$$T_{\mu\nu}(Q_1, Q_2) = T_{\mu\nu}(Q_1, Q_2) + T_{\nu\mu}(Q_2, Q_1), \quad (44)$$

where Q_1 and Q_2 are incoming photon momenta, $P = Q_1 + Q_2$ is the pseudoscalar's momentum, and the matrix element $T_{\mu\nu}(Q_1, Q_2)$ is given by

$$\begin{aligned} T_{\mu\nu}(Q_1, Q_2) &= \frac{\alpha_{em}}{\pi f_{\eta_{c(b)}}} \epsilon_{\mu\nu\alpha\beta} Q_{1\alpha} Q_{2\beta} G_{\gamma\gamma^* \eta_{c(b)}}(Q_1^2, Q_2^2) \\ &= \text{Tr} \int \frac{d^4 k}{(2\pi)^4} S(k_1) \Gamma_{\eta_{c(b)}}(P) S(k_2) i\Gamma_\mu(Q_2) S(k_3) i\Gamma_\nu(Q_1), \end{aligned} \quad (45)$$

where $k_1 = k - Q_1$, $k_2 = k + Q_2$, $k_3 = k$, and $\alpha_{em} = e^2/(4\pi)$. In order to conform with the experimental set up, the kinematic constraints are $Q_1^2 = Q^2$ and $Q_2^2 = 0$.

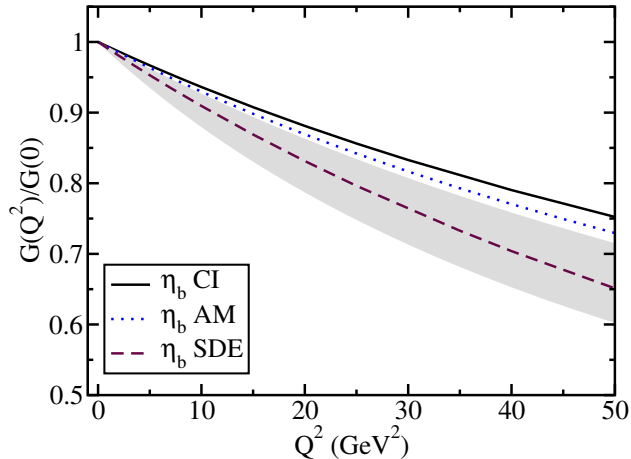


FIG. 5: CI results for the transition form factor for $\gamma\gamma^* \rightarrow \eta_b$ is represented by the (black) solid line. Blue (dotted) line stems from the AM, Eq. (20). (Grey) band corresponds to the NNLO nrQCD result taken from Ref. [66] (the band width expresses the sensitivity to the factorization scale). (Purple) dashed line is the full QCD calculation of Ref. [14]. As expected, AM does better than the CI in its connection with the QCD predictions, though the difference is not so conspicuous owing to the large mass of η_b .

We thus have $Q_1 \cdot Q_2 = -(m_{\eta_{c(b)}}^2 + Q^2)/2$, where $P^2 = -m_{\eta_{c(b)}}^2$.

interaction radius [fm]				
	Experiment	Lattice QCD	SDE	CI
η_c	0.166 [67]	0.141 [59]	0.16 [14]	0.133 [32]
η_b	—	—	0.041 [14]	0.040 [This work]

TABLE IX: Interaction radius of the transition $\gamma\gamma^* \rightarrow \eta_{c(b)}$ form factor as defined in Eq. (28). The experimental and lattice QCD results were extracted from their respective parametrization of data.

In Fig. 5, we present the CI results for the $\gamma\gamma^* \rightarrow \eta_{c(b)}$ TFF. Although not shown in Fig. 5, both TFFs have a pole at $Q^2 = -m_V^2$, as expected. For the η_c , the results compare fairly well with the *BABAR* data and Lattice QCD for low Q^2 ; see Ref. [32] for a more detailed analysis. However, for intermediate to large Q^2 , the CI provides a harder form factor, and the correct asymptotic Q^2 behavior is not captured; see also Fig. 6. We have neither experimental nor Lattice QCD data for the η_b TFF and interaction radius. However, we expect similar comparisons. Due to the same reason, in Fig. 5, we could only provide the comparison of our findings with the NNLO nrQCD result [66] and a recent QCD based computation in the SDE-BSE formalism [14]. Expectedly and encouragingly, our plots are in the same ballpark

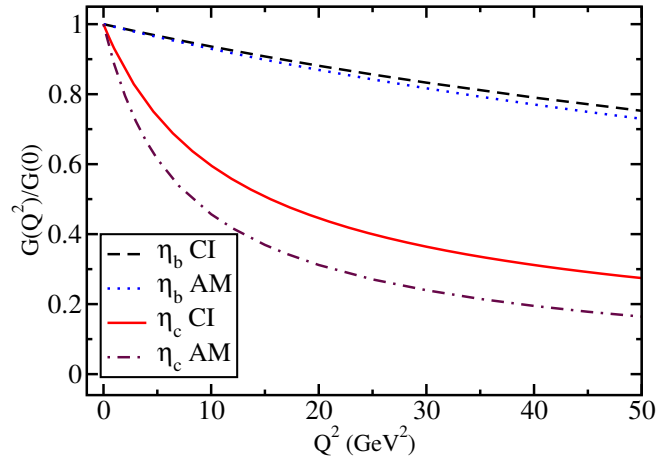


FIG. 6: Numerical results for $G(Q^2)$ for the transition $\gamma^*\gamma \rightarrow \eta_{c,b}$, normalized to its value at $Q^2 = 0$. We compare the results for the CI and the AM. (Red) solid line is for the η_c in the CI, compared to the (purple) dot-dashed line produced by the AM [32]. (Black) dashed curve is the CI prediction for the η_b , whereas the (blue) dotted line is the AM result. The distinction between each pair of comparative curves reduces substantially as the meson gets heavier.

despite the simplicity of the model.

On the other hand, in Fig. 6, we present our results for $G_{\gamma\gamma^*\eta_{c(b)}}$. From this figure and Fig. 5, it can be deciphered that both TFFs tend to a constant value for large Q^2 . However, the η_b TFF reaches this limit faster. The interaction radius of the η_c TFF, defined in Eq. (28) and tabulated in Table IX, compares well with Lattice QCD and the *BABAR* findings, as it probes the slope of the TFF for $Q^2 \rightarrow 0$. It is also in good agreement with a recent, more sophisticated, SDE result [14]. As with the η_c 's interaction radius, we expect to achieve similar agreement for the $\gamma\gamma^* \rightarrow \eta_b$ transition. Indeed our, result for r_{η_b} agrees nicely with that produced recently in Ref. [14]. We hope to have corresponding Lattice QCD and experimental input at some point in future.

VI. CONCLUSIONS

We compute the ground state spin-0 and spin-1 heavy quarkonia masses and decay constants by using a rainbow-ladder truncation of the simultaneous set of SDE and BSE within a CI model of QCD, developed initially for the light quarks sector [22–26].

It was realized in Ref. [31, 32] that the extension of the CI model to charmonia requires a reduction of the interaction strength and a corresponding increase in the ultraviolet cut-off. Present article is a generalization of this work to include bottomonia.

We find that the masses of the ground state heavy

quarkonia are in good agreement with experimental results available [50] as well as SDE calculations with QCD based refined truncations [10, 13]. The decay constants, however, are a bit lower. We have also computed the EFFs for η_c , η_b , J/Ψ , and Υ , the transition form factors of the η_c and η_b and the corresponding radii.

The dressing of the heavy-quark-photon vertex, consistent with the model truncation and the WTI, ensures that the form factors possess a vector meson pole at $Q^2 = -m_V^2$. However, since the vector meson mass is large, the effect of the meson vector pole on the charge radii is negligible. Our form factors, however, have better quantitative agreement with data and/or other calculations for small values of Q^2 , whenever available. They are harder for intermediate and large Q^2 . For the pseudoscalars, the both form factors tend to a constant for $Q^2 \rightarrow \infty$, which is a consequence of the momentum-independent interaction. On the other hand, the vector component of the vector meson is zero and the corresponding EFFs tend to behave as $1/Q^2$ for large Q^2 .

Our results for charge radii are in very good agreement with Lattice QCD data and experimental results, whenever available; furthermore comparison between the charge radii for charmonia and bottomonia confirms that the heavier the meson the closer it is to being a point

particle, justifying our reduction of the strength of the coupling.

All this is an encouraging first step towards a comprehensive study of heavy hadrons in this approach. Immediate next steps will involve flavored mesons and baryons. Our goal is to provide a unified description of light and heavy hadrons within the CI model.

VII. ACKNOWLEDGMENTS

The authors acknowledge financial support from CONACyT, México (doctoral scholarship for M.A. Bedolla; postdoctoral Contract No. 290917-UMSNH for J.J. Cobos-Martínez and research Grant No. CB-2014-242117 for A. Bashir). This work has also partly been financed by the CIC-UMSNH Grant 4.10. J.J. Cobos-Martínez also acknowledges the support of Conselho Nacional de Desenvolvimento Científico e Tecnológico (CNPq, Brazil), Grant No. 152348/2016-6 and Instituto Nacional de Ciência e Tecnologia - Física Nuclear e Aplicações (INCT-FNA, Brazil) CAPES: 88887.145710/2017-00.

-
- [1] J. J. Aubert et al. (E598), Phys. Rev. Lett. **33**, 1404 (1974).
 - [2] J. E. Augustin et al. (SLAC-SP-017), Phys. Rev. Lett. **33**, 1406 (1974), [Adv. Exp. Phys.5,141(1976)].
 - [3] S. W. Herb et al., Phys. Rev. Lett. **39**, 252 (1977).
 - [4] P. Jain and H. J. Munczek, Phys.Rev. **D48**, 5403 (1993), hep-ph/9307221.
 - [5] A. Krassnigg and P. Maris, J.Phys.Conf.Ser. **9**, 153 (2005), nucl-th/0412058.
 - [6] M. Bhagwat, A. Holl, A. Krassnigg, C. Roberts, and P. Tandy, Phys.Rev. **C70**, 035205 (2004), nucl-th/0403012.
 - [7] M. Bhagwat, A. Krassnigg, P. Maris, and C. Roberts, Eur.Phys.J. **A31**, 630 (2007), nucl-th/0612027.
 - [8] P. Maris and P. Tandy, Nucl.Phys.Proc.Suppl. **161**, 136 (2006), nucl-th/0511017.
 - [9] N. Souchlas, Phys.Rev. **D81**, 114019 (2010).
 - [10] M. Blank and A. Krassnigg, Phys.Rev. **D84**, 096014 (2011), 1109.6509.
 - [11] E. Rojas, B. El-Bennich, and J. de Melo, Phys.Rev. **D90**, 074025 (2014), 1407.3598.
 - [12] C. S. Fischer, S. Kubrak, and R. Williams, Eur. Phys. J. **A51**, 10 (2015), 1409.5076.
 - [13] M. Ding, F. Gao, L. Chang, Y.-X. Liu, and C. D. Roberts, Phys. Lett. **B753**, 330 (2016), 1511.04943.
 - [14] K. Raya, M. Ding, A. Bashir, L. Chang, and C. D. Roberts, Phys. Rev. **D95**, 074014 (2017), 1610.06575.
 - [15] P. Maris, AIP Conf.Proc. **892**, 65 (2007), nucl-th/0611057.
 - [16] A. Krassnigg, Phys.Rev. **D80**, 114010 (2009), 0909.4016.
 - [17] P. Maris and P. C. Tandy, Phys. Rev. **C62**, 055204 (2000), nucl-th/0005015.
 - [18] J. Chen, M. Ding, L. Chang, and Y.-x. Liu, Phys. Rev. **D95**, 016010 (2017), 1611.05960.
 - [19] N. Nakanishi, Phys. Rev. **130**, 1230 (1963).
 - [20] L. Chang, I. C. Cloet, C. D. Roberts, S. M. Schmidt, and P. C. Tandy, Phys. Rev. Lett. **111**, 141802 (2013), 1307.0026.
 - [21] K. Raya, L. Chang, A. Bashir, J. J. Cobos-Martínez, L. X. Gutiérrez-Guerrero, C. D. Roberts, and P. C. Tandy, Phys. Rev. **D93**, 074017 (2016), 1510.02799.
 - [22] L. Gutierrez-Guerrero, A. Bashir, I. Cloet, and C. Roberts, Phys.Rev. **C81**, 065202 (2010), 1002.1968.
 - [23] H. Roberts, C. Roberts, A. Bashir, L. Gutierrez-Guerrero, and P. Tandy, Phys.Rev. **C82**, 065202 (2010), 1009.0067.
 - [24] C. Chen, L. Chang, C. D. Roberts, S. Wan, and D. J. Wilson, Few Body Syst. **53**, 293 (2012), 1204.2553.
 - [25] H. L. Roberts, L. Chang, I. C. Cloet, and C. D. Roberts, Few Body Syst. **51**, 1 (2011), 1101.4244.
 - [26] H. Roberts, A. Bashir, L. Gutierrez-Guerrero, C. Roberts, and D. Wilson, Phys.Rev. **C83**, 065206 (2011), 1102.4376.
 - [27] A. Bashir, L. Chang, I. C. Cloet, B. El-Bennich, Y.-X. Liu, et al., Commun.Theor.Phys. **58**, 79 (2012), 1201.3366.
 - [28] G. Eichmann, R. Alkofer, I. Cloet, A. Krassnigg, and C. Roberts, Phys.Rev. **C77**, 042202 (2008), 0802.1948.
 - [29] I. Cloet, A. Krassnigg, and C. Roberts, eConf **C070910**, 125 (2007), 0710.5746.
 - [30] Y. Lu, C. Chen, C. D. Roberts, J. Segovia, S.-S. Xu, and H.-S. Zong, Phys. Rev. **C96**, 015208 (2017), 1705.03988.
 - [31] M. A. Bedolla, J. Cobos-Martínez, and A. Bashir, Phys. Rev. **D92**, 054031 (2015).

- [32] M. A. Bedolla, K. Raya, J. Cobos-Martinez, and A. Bashir, Phys. Rev. **D93**, 094025 (2016).
- [33] F. E. Serna, B. El-Bennich, and G. Krein, Phys. Rev. **D96**, 014013 (2017), 1703.09181.
- [34] C. D. Roberts, M. S. Bhagwat, A. Holl, and S. V. Wright, Eur. Phys. J. ST **140**, 53 (2007), 0802.0217.
- [35] A. Holl, C. D. Roberts, and S. V. Wright, in *20th Annual Hampton University Graduate Studies Program (HUGS 2005) Newport News, Virginia, May 31-June 17, 2005* (2006), nucl-th/0601071.
- [36] P. Maris and C. D. Roberts, Int. J. Mod. Phys. **E12**, 297 (2003), nucl-th/0301049.
- [37] R. Alkofer and L. von Smekal, Phys. Rept. **353**, 281 (2001), hep-ph/0007355.
- [38] I. G. Aznauryan et al., Int. J. Mod. Phys. **E22**, 1330015 (2013), 1212.4891.
- [39] P. Boucaud, J. Leroy, A. L. Yaouanc, J. Micheli, O. Pene, et al., Few Body Syst. **53**, 387 (2012), 1109.1936.
- [40] D. Binosi, C. Mezrag, J. Papavassiliou, C. D. Roberts, and J. Rodriguez-Quintero (2016), 1612.04835.
- [41] A. Deur, S. J. Brodsky, and G. F. de Teramond, Prog. Part. Nucl. Phys. **90**, 1 (2016), 1604.08082.
- [42] D. Ebert, T. Feldmann, and H. Reinhardt, Phys.Lett. **B388**, 154 (1996), hep-ph/9608223.
- [43] C. Roberts, Prog.Part.Nucl.Phys. **61**, 50 (2008), 0712.0633.
- [44] R. Farias, G. Dallabona, G. Krein, and O. Battistel, Phys.Rev. **C73**, 018201 (2006), hep-ph/0510145.
- [45] R. Farias, G. Dallabona, G. Krein, and O. Battistel, Phys.Rev. **C77**, 065201 (2008), hep-ph/0604203.
- [46] F. Gross, *Relativistic quantum mechanics and field theory* (Wiley, New York, 1993), 1st ed.
- [47] E. E. Salpeter and H. A. Bethe, Phys. Rev. **84**, 1232 (1951).
- [48] M. Gell-Mann and F. Low, Phys. Rev. **84**, 350 (1951).
- [49] P. Maris, C. D. Roberts, and P. C. Tandy, Phys. Lett. **B420**, 267 (1998), nucl-th/9707003.
- [50] K. Nakamura and P. D. Group, Journal of Physics G: Nuclear and Particle Physics **37**, 075021 (2010), URL <http://stacks.iop.org/0954-3899/37/i=7A/a=075021>.
- [51] F. F. Mojica, C. E. Vera, E. Rojas, and B. El-Bennich, Phys. Rev. **D96**, 014012 (2017), 1704.08593.
- [52] C. T. H. Davies, C. McNeile, E. Follana, G. P. Lepage, H. Na, and J. Shigemitsu, Phys. Rev. **D82**, 114504 (2010), 1008.4018.
- [53] G. C. Donald, C. T. H. Davies, R. J. Dowdall, E. Follana, K. Hornbostel, J. Koponen, G. P. Lepage, and C. McNeile, Phys. Rev. **D86**, 094501 (2012), 1208.2855.
- [54] A. Krassnigg, M. Gomez-Rocha, and T. Hilger, J. Phys. Conf. Ser. **742**, 012032 (2016), 1603.07232.
- [55] C. McNeile, C. T. H. Davies, E. Follana, K. Hornbostel, and G. P. Lepage, Phys. Rev. **D86**, 074503 (2012), 1207.0994.
- [56] B. Colquhoun, R. J. Dowdall, C. T. H. Davies, K. Hornbostel, and G. P. Lepage, Phys. Rev. **D91**, 074514 (2015), 1408.5768.
- [57] P. Maris and C. D. Roberts, Phys. Rev. **C56**, 3369 (1997), nucl-th/9708029.
- [58] P. Maris and P. C. Tandy, Phys. Rev. **C60**, 055214 (1999), nucl-th/9905056.
- [59] J. J. Dudek, R. G. Edwards, N. Mathur, and D. G. Richards, J.Phys.Conf.Ser. **69**, 012006 (2007).
- [60] P. Maris and P. C. Tandy, Phys. Rev. **C61**, 045202 (2000), nucl-th/9910033.
- [61] M. S. Bhagwat and P. Maris, Phys. Rev. **C77**, 025203 (2008), nucl-th/0612069.
- [62] Y. Li, P. Maris, and J. P. Vary, Phys. Rev. **D96**, 016022 (2017), 1704.06968.
- [63] J. J. Dudek, R. G. Edwards, and D. G. Richards, Phys. Rev. **D73**, 074507 (2006), hep-ph/0601137.
- [64] R. G. Arnold, C. E. Carlson, and F. Gross, Phys. Rev. **C21**, 1426 (1980).
- [65] S. J. Brodsky and J. R. Hiller, Phys. Rev. **D46**, 2141 (1992).
- [66] F. Feng, Y. Jia, and W.-L. Sang, Phys. Rev. Lett. **115**, 222001 (2015), 1505.02665.
- [67] V. P. Druzhinin (BaBar), PoS **ICHEP2010**, 144 (2010), 1011.6159.